J Comput Neurosci (2008) 25:158–168
DOI 10.1007/s10827-007-0070-6

Mechanism of gain modulation at single neuron and network levels

M. Brozović · L. F. Abbott · R. A. Andersen

Received: 12 February 2007 / Revised: 17 November 2007 / Accepted: 3 December 2007 / Published online: 23 January 2008

Abstract Gain modulation, in which the sensitivity of a neural response to one input is modified by a second input, is studied at single-neuron and network levels. At the single neuron level, gain modulation can arise if the two inputs are subject to a direct multiplicative interaction. Alternatively, these inputs can be summed in a linear manner by the neuron and gain modulation can arise, instead, from a nonlinear input–output relationship. We derive a mathematical constraint that can distinguish these two mechanisms even though they can look very similar, provided sufficient data of the appropriate type are available. Previously, it has been shown in coordinate transformation studies that artificial neurons with sigmoid transfer functions can acquire a nonlinear additive form of gain modulation through learning-driven adjustment of synaptic weights. We use the constraint derived for single-neuron studies to compare responses in this network with those of another network model based on a biologically inspired transfer function that can support approximately multiplicative interactions.

Keywords Gain modulation · Neural noise · Tuning curves · Power law

Action Editor: Nicolas Brunel

M. Brozović (✉) · R. A. Andersen
Division of Biology, Mail Code 216-76,
California Institute of Technology,
Pasadena, CA 91125, USA
e-mail: brozovic@vis.caltech.edu

L. F. Abbott
Center for Neurobiology and Behavior
Department of Physiology and Cellular Biophysics,
Columbia University College of Physicians and Surgeons,
New York, USA

1 Introduction

Gain modulation is defined as a change in the sensitivity of a neuronal response to one set of inputs that depends on the activity of a second set of inputs. It was first observed in neurons of the parietal cortex of the macaque monkey that combine retinal and gaze signals in a multiplicative manner (Andersen and Mountcastle 1983; Andersen 1985). Since then, gain modulation has been seen in other cortical areas (Galletti and Battaglini 1989; Bremmer et al. 1997; Salinas and Sejnowski 2001) and found to involve not only sensory but also cognitive inputs such as those representing states of attention (Salinas and Abbott 1997; Treue and Martinez-Trujillo 1999; McAdams and Maunsell 2000). Furthermore, gain modulation has come to be viewed as a major computation principle of nonlinear neuronal processing (Salinas and Thier 2000).

A number of cellular mechanisms have been proposed that allow neurons to combine two sets of inputs in a directly multiplicative manner (Mel 1993; Doiron et al. 2001; Chance et al. 2002; Gabbiani et al. 2002; Mitchell and Silver 2003; Prescott and De Konick 2003). However, as Murphy and Miller (2003) have pointed out, gain modulation can also arise from a nonlinear dependence of the input current on stimulus parameters followed by a nonlinear f–I curve describing the relationship between neuronal firing rate and input current. We call this second form of gain modulation nonlinear additive. Normalization, which has been used in models of visual cortex (Heeger 1992; Schwartz and Simoncelli 2001), might be considered another form of gain modulation, but we lump it together with the directly multiplicative forms we study.

Gain modulation can be studied at both the single-neuron and network levels. We begin our investigation at the single neuron level where distinguishing nonlinear additive and directly multiplicative mechanisms of gain

modulation on the basis of extracellular recordings can be difficult (Murphy and Miller 2003), especially if *f–I* curves are described by power-law functions (Murthy et al. 1988; Albrecht and Geisler 1991; Carandini et al. 1997; Gardner et al. 1999; Carandini and Ferster 2000). To address this issue, we derive a mathematical constraint satisfied by directly multiplicative gain modulation and look to see when a nonlinear additive mechanism might come close to satisfying this constraint. This is followed by an examination of how experimental data can be analyzed to distinguish between directly multiplicative and nonlinear additive mechanisms by determining if the constraint is satisfied. For brevity, we sometimes refer to the nonlinear additive and directly multiplicative cases as NA and DM, respectively.

We next address gain modulation at the network level. In previous studies, gain modulation has simply been imposed upon a network by fiat (Pouget and Sejnowski 1995; Salinas and Abbott 1996), or it has arisen in network models as a consequence of learning rules that adjust the strengths of synaptic connections in order to make the network perform a particular task (Zipser and Andersen 1988; Xing and Andersen 2000; Smith and Crawford 2005). In the latter case, the individual neurons had transfer functions, the neural network analog of *f–I* curves, that were sigmoidal and allowed nonlinear additive, but not directly multiplicative, gain modulation to arise. In addition to this classical sigmoid transfer function, we consider a biologically inspired *f–I* curve (Abbott and Chance 2005) that can support an approximation of direct multiplication. However, this alternative model is not purely multiplicative and, as we will see, it supports a nonlinear additive form of gain modulation as well. Both models are studied in the context of a coordinate transformation network. We apply the mathematical constraint derived for the single-neuron computation to these two biophysical models to determine whether they are implementing distinct additive and multiplicative mechanisms.

2 Methods

To study nonlinear additive and directly multiplicative gain modulation mechanisms, we construct both single-neuron and network models, which are described in the following two subsections. A third subsection describes the analysis methods we use.

2.1 Single-neuron models

The single-neuron models we study are descriptions of the neural responses rather than biophysical models. The models are constructed from response functions and noise, as discussed in the follow two subsections.

Response functions Figure 1 shows responses of model neurons that illustrate the similarities and differences between nonlinear additive and directly multiplicative gain modulation. For Fig. 1(a) and (b), which is an NA example, the neuronal response plotted is given by $R(x,y) = c(f(x) + g(y))^{3.4}$, with $f(x) = a_1 \exp\left(-x^2/a_2^2\right)$, $g(y) = b_1 y + b_2$, and $c = 0.02$, $a_1 = 4$, $a_2 = 1.5$, $b_1 = -1$, and $b_2 = 2$. Figure 1(c) and (d) shows a DM neuron with the firing rate calculated as $R(x,y) = f(x)g(y)$, with $f(x)$ and $g(y)$ given as above, except that $a_1 = 10$, $a_2 = 0.9$, $b_1 = -0.5$, and $b_2 = 1$. Figure 1(e) and (f) shows an NA neuron that, once again, has a response given by $R(x,y) = c(f(x) + g(y))^{3.4}$, but with $f(x) = a_1 \tanh(x) + a_2$, $g(y) = b_1 y + b_2$, and $a_1 = 1$, $a_2 = 1$, $b_1 = 0.5$, and $b_2 = 0$. The DM neuron for Fig. 1(g) and (h) has $R(x,y) = f(x)g(y)$, with these same $f(x)$ and $g(y)$ except that $b_2 = 1$.

Neural noise To generate more realistic neuronal responses than the smooth mathematical functions from Fig. 1, we used three noise sources. The first noise model used the tuning curves from Fig. 1 as firing rates for a Poisson process, $\lambda = R(x,y)$. The response field was generated a number of times, and the average response was used as simulated data. The second model used a normal noise distribution with mean $\mu(x,y) = R(x,y)$ and standard deviation $\sigma(x,y) = \sqrt{R(x,y)}$. Because the firing rates we used were fairly large, this second model was practically indistinguishable from the Poisson process (except at the boundaries of the tuning curves). A third model used a lower variance normal distribution with $\sigma(x,y) = \sqrt{R(x,y)/2}$.

2.2 Network models

The networks we construct perform a simple coordinate transformation. We consider a case were the position of an auditory target is initially encoded in head-centered coordinates and needs to be converted to an eye-centered reference frame (Grunewald et al. 1999; Cohen and Andersen, 2000; Groh et al. 2001). In this task, x corresponds to an angle that defines the location of the auditory target relative to the head, and y is an angle that represents the gaze direction of the eyes relative to the head. We model neuronal responses in such a task using a feedforward network (Bishop 1995) that consists of three layers of processing units: an input layer with responses that separately represent x and y, a hidden layer that generates a combined representation of these two inputs, and an output layer that represents the result of the coordinate transformation which, in this case, is the difference of the two input angles, $x–y$.

Input and output layers The input layer represents x and y in two separate maps producing the outputs $f_i(x)$ and $g_j(y)$

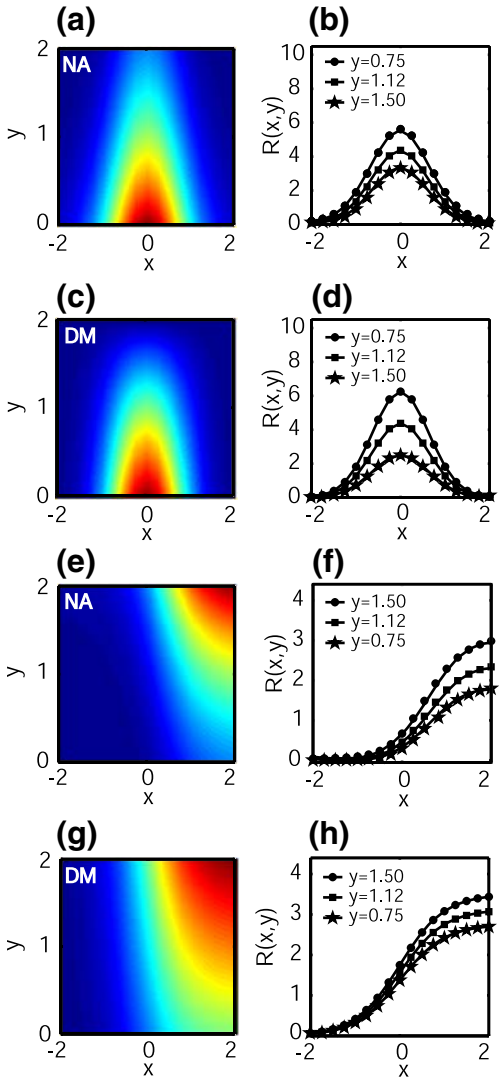

Fig. 1 Comparison of nonlinear additive and directly multiplicative neural responses, with R in arbitrary units. The two input functions are a Gaussian (**a**–**d**) or a sigmoidal (**e**–**h**) $f(x)$ encoding the position of a stimulus (e.g. retinal position) and a linear $g(y)$ encoding a modulatory parameter (e.g. gaze angle). (**a**) Response field of a neuron that performs input addition followed by a nonlinear transfer function. The transfer function is a power law (the 3.4 power). (**b**) Tuning curves from (**a**) for three different values of the modulatory parameter y. *Solid lines* show a scaled Gaussian fit. (**c**) Response field of a neuron that performs direct multiplication of its two input functions. (**d**) Tuning curves from (**c**) for different values of the parameter y. *Solid lines* show $f(x)$ scaled by $g(y)$. (**e**) Response field of a neuron that performs input addition followed by a power law transfer function, but for a sigmoid rather than Gaussian $f(x)$. The transfer function is again a power law (the 3.4 power). (**f**) Tuning curves from (**e**) for three different values of y. (**g**) Response field of a neuron that performs direct multiplication of the two input functions. (**h**) Tuning curves from (**g**) for different values of the parameter y. The *solid lines* in (**f**) and (**h**) show $f(x)$ scaled by $g(y)$

in neurons i and j, respectively. The map for x consists of eight units that encode the location of the auditory target relative to the head. The response of each unit is modeled as a Gaussian with a width of 15°. The angle that produces the maximum response in these Gaussian units is assigned to one of eight uniformly distributed locations between −35° and +35°. This network is based on average tuning curves, so it does not include noise. The second map represents y, the eye position in head-centered coordinates (the gaze direction). This map is constructed from units with responses that are sigmoid functions of y, eight units with positive slopes and eight with negative slopes. Each set of eight sigmoids spans the space from −35° to +35°, in increments of 10°. The slope parameter for the sigmoids is 8°. The outputs from these input layer units are then fed to a variable number (usually 20) of hidden layer units and from there to the 8 output units.

Network architecture Neurons in the first network we consider incorporate a nonlinear additive mechanism, and the responses of hidden layer (R) and output layer (T) neurons are determined by the following equations:

$$\begin{aligned} R_k &= F(I_k), \quad I_k = w^1_{ik} f_i(x) + \sum_j w^2_{jk} g_j(y) \\ T_m &= F(I_m), \qquad I_m = \sum_k w^3_{km} R_k(I_k) \end{aligned} \tag{1}$$

where I_k and I_m involve weighted sums over all presynaptic units, w^1_{ik} and w^2_{jk} are weight matrices that determine how much the input unit responses $f_i(x)$ and $g_j(y)$ contribute to the activation of hidden unit k, $R_k(I_k)$. The sum involving w^3_{km} determines the activation of output unit m, $T_m(I_m)$. F denotes the sigmoidal nonlinearity, $F(I) = 1/(1+\exp(-I))$, used as the input–output transfer function.

The second network we study is built from units that compute not only on the basis of the total presynaptic input I (defined as in Eq. (1)), but also depend on the input variance σ,

$$\begin{aligned} R_k &= F(I_k, \sigma_k), \quad \sigma^2_k = \sum_i \left(w^1_{ik} f_i(x)\right)^2 + \sum_j \left(w^2_{jk} g_j(y)\right)^2 \\ T_m &= F(I_m, \sigma_m), \qquad \sigma^2_m = \sum_m \left(w^3_{km} R_k(I_k)\right)^2 \end{aligned} \tag{2}$$

where the transfer function (Abbott and Chance 2005) is

$$F(I,\sigma) = \frac{I - \sigma - c_1}{1 - \exp(-c_2(I - \sigma - c_1)/(\sigma + c_1))} \tag{3}$$

with c_1 and c_2 constants. These units allow for both nonlinear additive and directly multiplicative interactions, at least over some part of their response range. The equations on the right side of Eq. (2) define what we mean by the term input variance. Our equation for the variance assumes non-Poissonian contributions.

Network training Both networks were trained by applying standard backpropagation (Rumelhart et al. 1986) with a gradient descent algorithm (Bishop 1995) to their weights (calculating Δw). The weights were adjusted in increments determined by a learning rate $\lambda\,(w \rightarrow w + \lambda\,\Delta w)$. The network with sigmoid nonlinearity was trained with λ= 0.05, while the network with the nonlinearity defined by Eq. (3) had λ=0.005.

The goal of training was to make the eight output units of the network match the responses given by eight Gaussian functions of the difference of the input variables (x–y). The centers of these target Gaussians spanned the eye-centered space from −35° to +35°. The width of the Gaussians was 15°. Performance was judged by computing the sum of the squared errors between the network responses and the target responses given by the Gaussian functions. We considered a network well trained when the error dropped to 0.0040. This corresponds to a 3% error on the amplitude of the Gaussians, a 0.6° error on the position of the maximum of the Gaussians, or a 0.7° error on the width of the Gaussians.

Training consisted of presenting 100 combinations of the two input variables: the location of an auditory target with respect to the head and the gaze angle. The input space from −45° to +45° was randomly sampled in steps of 2°. This resulted in a large number of input combinations for target and eye positions. The training set was optimized by keeping only the input combinations that produced an output variable (Sound in Eye=Sound in Head−Eye in Head) in the range between −45° and +45°. The weights between the layers were initially set to small (positive and negative) random values. As the network trained, the weights were adjusted to minimize the error by stochastic gradient descent.

2.3 Analysis methods

Central difference equation To calculate the first numerical derivative of a neuron's response function $R(x,y)$ at point $\left(x+\frac{\Delta x}{2}, y\right)$ we used the central difference formula:

$$R'_x = \frac{\mathrm{d}R}{\mathrm{d}x}\left(x+\frac{\Delta x}{2}, y\right) = \frac{R(x+\Delta x, y) - R(x,y)}{\Delta x} + O\left((\Delta x)^2\right), \tag{4a}$$

where Δx is the size of the grid, and O is the error term which is proportional to $(\Delta x)^2$. An equivalent formula may be written for the derivative over y. The second derivative at point $\left(x+\frac{\Delta x}{2}, y+\frac{\Delta y}{2}\right)$ is then:

$$R''_{xy} = \frac{d^2R}{dxdy}\left(x+\frac{\Delta x}{2}, y+\frac{\Delta y}{2}\right) \approx \frac{\frac{dR}{dx}\left(x+\frac{\Delta x}{2}, y+\Delta y\right) - \frac{dR}{dx}\left(x+\frac{\Delta x}{2}, y\right)}{\Delta y} \tag{4b}$$

Wilcoxon signed ranks test To quantify result from our test using noisy "data" of whether a response field comes from a nonlinear additive or directly multiplicative mechanism, we make use of a Wilcoxon signed ranks test. This nonparametric method was used to determine if the median of the normalized distance between the firing rate and the constraint we used (defined in Section 3) differs significantly from 0. The test gives the probability r of observing a result equal to or larger than that obtained from the data. Values of r<0.05 led to rejection of the null hypothesis that the interaction was directly multiplicative.

3 Results

The results are divided into two parts. In the first part, we address the shapes of the response fields and gain properties of single neurons. In the second part, we study how two different transfer functions give rise to approximate gain modulation in the hidden-layer units of a network model.

3.1 Gain modulation at the single-neuron level

Consider a neuron that receives input from two sources that are characterized by two stimulus parameters x and y (e.g. the auditory target position and gaze direction of the eyes). These inputs are represented by afferent firing rates that are functions of these parameters, $f(x)$ for the afferents carrying information about the parameter x and $g(y)$ for the afferents responding to y. In general, the firing rate of a postsynaptic neuron driven by these inputs, labeled by R, will be some function of $f(x)$ and $g(y)$. Directly multiplicative gain modulation occurs when the postsynaptic firing rate is a product of two factors, $R(x,y)=f(x)g(y)$. We denote these two factors by $f(x)$ and $g(y)$, but these denote generic functions that do not have to be identical to the function used to describe the inputs. In the multiplicative case, the "tuning curve" of the neuronal firing rate (R plotted as a function of x) is multiplicatively scaled by the value of $g(y)$, which is how gain modulation was originally defined. Nonlinear additive gain modulation occurs when $R(x,y)=F(f(x)+$

g(y)). Given that the functions $f(x)$, $g(y)$ and F are, at this point, arbitrary, how can we distinguish these two cases?

Before addressing this question, we show, following (Murphy and Miller 2003), that these two computationally different expressions can produce very similar response fields and similar gain modulation. Figure 1 shows two-dimensional ($R(x,y)$ plotted as a function of x and y) and one-dimensional ($R(x,y)$ plotted as a function of x for three different y values) response fields for the nonlinear additive [Fig. 1(a,b,e,f)] and directly multiplicative [Fig. 1(c,d,g,h)] cases. The neurons in Fig. 1(a–d) have a Gaussian function for $f(x)$ whereas $f(x)$ is sigmoidal in Fig. 1(e–h), and both have linear functions for $g(y)$ and $F(z)=z^{3.4}$ (as in Murphy and Miller 2003). Panels b, d, f, and h show that similar response fields can be obtained whether the neuron is performing nonlinear addition (panels b and f) or direct multiplication (panels d and h) of its two inputs (provided that the parameters defining these response functions are chosen appropriately).

Mathematical constraint Although they can be hard to distinguish, the directly multiplicative ($R(x,y)=f(x)g(y)$) and nonlinear additive ($R(x,y)=F(f(x)+g(y))$) cases are mathematically distinct. A useful way to reveal this distinction is to compare the product of the x and y derivatives of $R(x,y)$ with the mixed second-derivative through the ratio:

$$G=\left(\frac{\partial R}{\partial x}\right)\left(\frac{\partial R}{\partial y}\right)\Big/\left(\frac{\partial R}{\partial x\partial y}\right). \tag{5}$$

A bit of algebra reveals that, in the directly multiplicative case, G is constrained to be equal to R ($G=R$). In the nonlinear additive case, $G=\left(F'\right)_2/F''$, where the primes denote derivatives with respect to $f(x)$ and $g(y)$. Because the firing rate is given by $R=F$, the nonlinear additive firing rate will look like the directly multiplicative rate if $G=\left(F'\right)^2/F''\approx R=F$ or, equivalently, if $\left(F'\right)^2/F''\approx F$.

There is a firing-rate dependence that satisfies the condition $\left(F'\right)^2/F''=F$ exactly, the exponential. This is obviously a function that makes it impossible to distinguish the two cases because the exponential of a sum is the product of the exponentials. If F is a power-law function, $F=z^p$, then $\left(F'\right)^2/F''=p^2F/(p(p-1))$. Thus, the power-law additive mechanism will look similar to the multiplicative case if $p^2\approx p(p-1)$, which is satisfied if p is sufficiently large. For this reason, we consider a power-law form for F in our analysis of single-neuron responses, even though the analogous F in our network model is sigmoidal. Portions of the sigmoidal curve can be approximated by a power-law function but, more importantly, using a power-law for our single-neuron studies allows us to consider what amounts to a worst-case situation.

The constraint $G=R$ that we consider is, of course, not the only way of distinguishing the directly multiplicative and nonlinear additive cases. We use it because it has the advantage of providing a test that only requires us to plot and evaluate a function of one variable, R, and test whether or not $G=R$. In other words, rather than having to examine three-dimensional plots of a constrained quantity as a function of x and y, we can simply examine two-dimensional plots of G vs R. In the multiplicative case, the function $R(x,y)$ evaluated over a grid of points is a matrix of rank 1, and tests of this feature can be used as a indicator of a multiplicative form. However, in realistic examples, we only expect a multiplicative form to apply over a range of R values, and the rank test provides only a global measure. The constraint we use, allows us to evaluate the nature of the input interaction as a function of firing rate.

Testing the constraint on response fields of single neurons We do not believe that existing data can distinguish the directly multiplicative and nonlinear additive cases, so we now consider what type and amount of data would be needed for this purpose. We consider two problems associated with real data: finite stimulus resolution and variability.

We compare the computed G with the value of the firing rate R, over a range of rates, to see if the constraint $G=R$ is satisfied, using the model results from Fig. 1 as surrogate data. We consider x range from −2 to 2 and y range from 0 to 2, both in steps $\Delta x=0.5$ and $\Delta y=0.5$. The comparisons, for the neural responses shown in Fig. 1, are shown in Fig. 2. The directly multiplicative (panels b and d) and nonlinear additive (panels a and c) cases can easily be distinguished. Figure 2 illustrates that G values for the directly multiplicative cases lie exactly on the diagonal, whereas those for the nonlinear additive cases lie above the diagonal. This latter feature is due to the fact that $G=pF/(p-1)$ for that case, and $G=p/(p-1)>1$ for positive p. The R vs G plot appears to have half as many points for the Gaussian response fields as for the sigmoidal field because Gaussian field is symmetric, so half the points overlap.

The Wilcoxon test was applied to quantify the statistical significance of the hypothesis that $G=R$. We removed parts of the response field with low or no activity by imposing the threshold condition . This removed part of the NA region where multiplication is mimicked quite successfully (in particular, the low firing region of the sigmoid NA). The r values in Fig. 2 and subsequent figures give the probabilities for accepting the null hypothesis of a multiplicative interaction.

Calculating G over an 8×4 grid of points requires a total of $9\times5+8\times5+9\times4+8\times4=153$ measurements of the single response field. This can be done for a

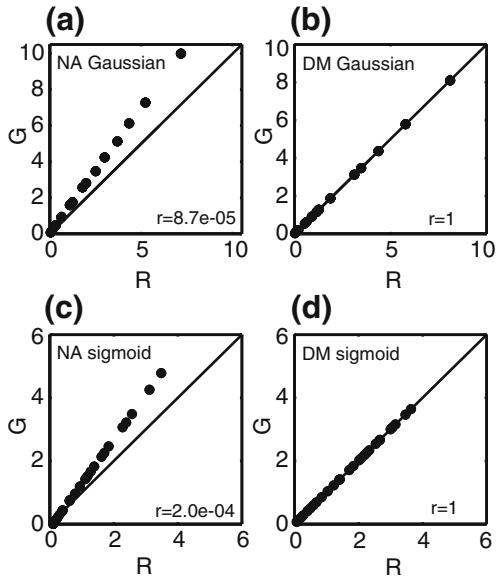

Fig. 2 Testing the mathematical constraint. The *black circles* are the derivative ratios, G of Eq. (5) calculated at different points of the response field and plotted as a function of the rate. (**a**) G vs R for the response field of Fig. 1(a). (**b**) G vs R for the response field of Fig. 1(c). (**c**) G vs R for the response field of Fig. 1(e). (**d**) G vs R for the response field of Fig. 1(g). Wilcoxon r values give probabilities for accepting the null hypothesis of a multiplicative interaction

mathematical model, but would it be applicable in the real experimental conditions with noisy measurement and much lower data resolution? Figure 3(a) and (f) show two Gaussian response fields from Fig. 1(a) and (c) as they would look from a 9×5 grid of measurements. All the other R values needed for the numerical calculation of derivatives [Eqs. 4(a) and 4(b)] were obtained by triangle based linear interpolation of the "measured" data (*griddata* function in Matlab). Amplitudes were scaled 10 times to correspond to a maximum firing rate of 89 Hz. Figure 3(b) and (g) shows an 8×4 grid of G vs R (at points $x+\frac{\Delta x}{2}, y+\frac{\Delta y}{2}$) as would be obtained from this limited data without noise.

We now explore the effects of simulated neuronal response variability on the applicability of the derived constraints for real data. Given a reasonable number of experimental trials and a realizable x–y grid, is it still possible to distinguish between direct multiplication and nonlinear addition? Figure 3(c) and (h) show simulated data assuming a Poisson process as described in the Methods. We had to average 15 trials for each point in a 9×5 grid of x and y stimuli for the derived constraints to become consistently visible as off-diagonal scattering (Wilcoxon, $r<0.05$). The same is true for noisy data generated from a normal distribution [Fig. 3(d) and (i)]. The last two plots [Fig. 3(e) and (j)] have variance reduced by a factor of 2. In general, experiments could be designed with multiple stimuli presented in a single trial, for example, if three auditory targets were presented per single eye fixation. This would require only $9\times5\times15/3\approx225$ trials, an achievable goal. By comparison, (Murphy and Miller 2003) suggested that the distinction between the directly multiplicative and nonlinear additive cases will require experimental data precise enough so that increases or decreases of tuning curve width on the order of 10–20% can be detected.

In Fig. 4, we explore the effect of discrete grids and noise on the sigmoidal response fields from Fig. 1(e) and (g). Figure 4(a) and (f) shows the response fields obtained from a limited number of measurements (9×5), scaled to a maximum of 165 Hz. Again, we used linear interpolation (*griddata* in Matlab) for other x,y locations. R vs G plots in Fig. 4(b) and (g) clearly show the difference between the NA and DM cases, as verified by the Wilcoxon r values. A consistent (90%) detection of the off-diagonal behavior in the noisy measurements required 100 trials per each of the 9×5 (x,y) points. Figure 4(c) and (h) show results for noisy response fields corresponding to the Poisson noise model, while Fig. 4(d) and (i) show the same for the normal distribution. Figure 4(e) and (j) are the results for the normal noise reduced by a factor of $\sqrt{2}$.

Figure 5 shows the summary of potential number of trials with respect to the type of noise in the data. The measurement resolution grid is always 9×5, used to interpolate and calculate R vs G at 8×4 points. Figure 5(a) summarizes how the efficiency of detecting the off-diagonal R vs G scattering (indicating NA) changes with respect to the type of noise and number of trials at each of the 8×4 (x,y) points. The circles indicate efficiencies for detecting true NA [as in Fig. 3(a)]. The squares indicate misidentification of DM responses [as in Fig. 3(f)] as NA. Each circle (and square) was calculated based on 100 random initializations for a particular type of noise (normal (n), normal reduced by $\sqrt{2}$ ($n2$) and Poisson (p)). Each initialization gave an R vs G plot that was categorized with Wilcoxon criteria as on- or off-diagonal ($r<0.05$) for $R > 0.1\,R_{\max}$. Different lines follow how the efficiency changes for each type of noise with respect to number of trials used. Obviously, the cases with the smallest noise ($n2$) require the fewest number of trials to correctly identify the true NA neuron. There were very few false positives (squares) under all conditions because noise symmetrically scatters points about the diagonal.

Figure 5(b) is equivalent to Fig. 5(a), but for the sigmoidal responses from Fig. 4. This response field shape requires higher number of trials to detect the off-diagonal scattering, primarily because it departs slowly from the diagonal, and it also has a well matched diagonal part. This is enough to influence the Wilcoxon test. Seeing a clear off-diagonal trend for detecting this type of NA response field would require $9\times5\times100=4{,}500$ trials per RF, a formidable task, unless the number of trials is reduced by multiple target presentations (4,500/3= 1,300 trials).

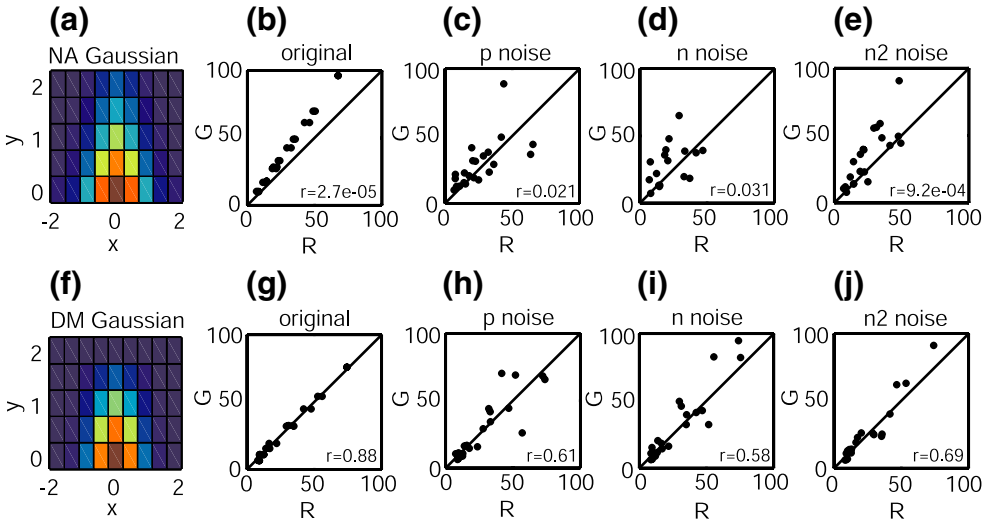

Fig. 3 (**a**) NA Gaussian neuron from Fig. 1(a), scaled 10 times (maximum firing rate of 89 Hz) as seen on a 9×5 grid of measurements. (**b**) G vs R plot shows 8×4 points computed from finite-difference derivatives of the responses in **a** with no noise. (**c**) G vs R plot for the response field in (**a**) obtained from 15 noisy measurements generated by a Poisson (p) process. (**d**) Same as (**c**), but the noisy measurements were generated from a normal (n) distribution with a standard deviation equal to the square of the firing rate calculated for each point. (**e**) Same as (**d**), but with the noise reduced by $\sqrt{2}$ ($n2$). (**f**) DM Gaussian neuron from Fig. 1(c), scaled 10 times, as seen on a 9×5 grid of measurements. (**g**) G vs R plot has 8×4 points computed from the response field of (**f**) as in (**b**). (**h**) G vs R plot obtained from 15 noisy (Poisson) measurements of the response field in (**g**). (**i**) G vs R plot calculated from 15 noisy (normal distribution) measurements. (**j**) G vs R plot based on average of 15 trials in reduced noise case (normal distribution with the noise reduced by $\sqrt{2}$. Wilcoxon r values give probabilities for accepting the null hypothesis of a multiplicative interaction

3.2 Gain modulation at the network level

As stated in the Introduction, gain modulation has been studied in network models associated with coordinate transformations. The most straightforward approach is to construct a network from neurons that are simply postulated to perform direct multiplication (Pouget and Sejnowski 1995; Salinas and Abbott 1996). However, we are interested in the multilayer feedforward networks (Zipser and Andersen 1988; Xing and Andersen 2000; Smith and Crawford

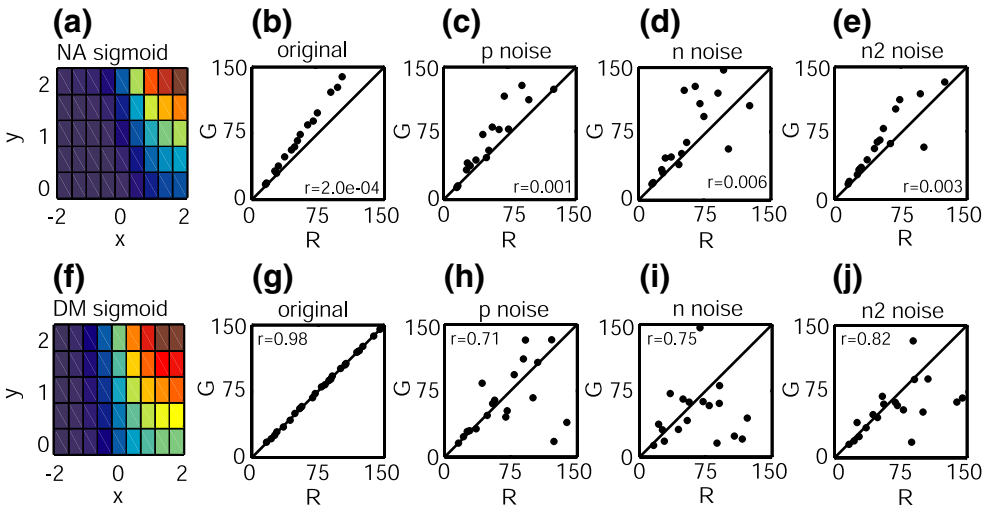

Fig. 4 (**a**) Response field of NA sigmoidal neuron from Fig. 1(e), scaled 40 times (maximum firing rate of 165 Hz) as seen on a 9×5 grid of data. (**b**) G vs R plot for the response field results in 8×4 data points. (**c**) G vs R plot calculated from the response field in (**a**), averaged over 100 noisy (Poisson (p)) measurements. (**d**) G vs R plot calculated from the response field in (**a**) averaged over 100 noisy (normal distribution (n)) measurements. (**e**) Same as in (**d**), but with the noise reduced by $\sqrt{2}$ ($n2$). (**f**) Response field of DM sigmoidal neuron from Fig. 1(g), scaled 40 times, as seen over a 9×5 grid. (**g**) Resulting 8×4 derivative data points shown in a G vs R plot. (**h**) G vs R plot based on 100 trials with Poisson noise. (**i**) G vs R plot based on 100 measurements with normally distributed noise. (**j**) Same as in (**i**), but with reduced normal noise and 100 trials. Wilcoxon r values give probabilities for accepting the null hypothesis of a multiplicative interaction

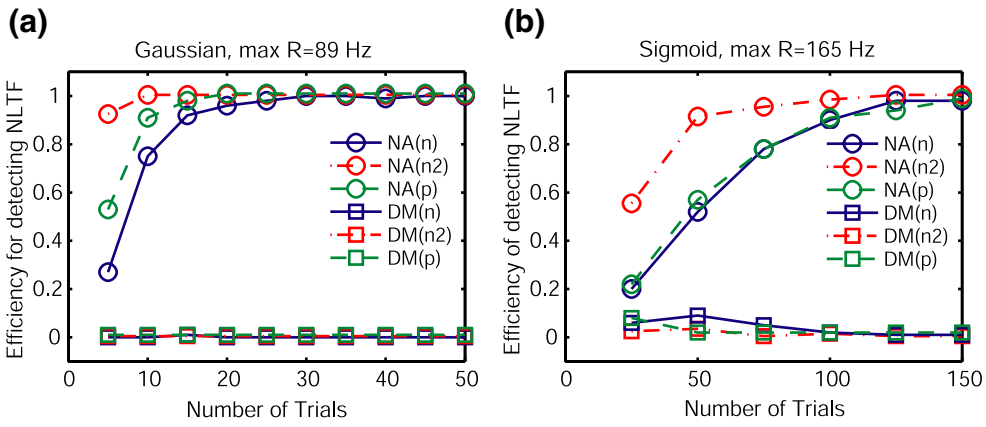

Fig. 5 (**a**) Efficiency for detecting off-diagonal behavior of a Gaussian neuron for various types of noise (normal (*n*), reduced normal (*n*2) and Poisson (*p*)) and number of trials. *Circles* denote efficiency of detecting NA transfer functions. *Squares* denote false identification of DM Gaussian neuron as NA neuron. (**b**) Same as in (**a**) only for the sigmoidal response field neurons. Firing rates are in arbitrary units

2005) where the (approximate) gain modulation arises as a consequence of weight adjustment.

3.3 Transfer functions and their effects on gain modulation

We construct and compare two feedforward networks with the general architecture described in the Methods. The networks differ in the type of transfer functions used. For the sigmoid transfer (ST) network, we used a sigmoidal transfer function that supports additive nonlinear gain modulation, as used in the standard Zipser–Andersen model (1988). For the second case, we consider a more complex nonlinear transfer function. It has been shown previously that *f*–*I* curves can scale almost multiplicatively through the effects of input variance (Doiron et al. 2001; Chance et al. 2002; Mitchell and Silver 2003; Prescott and De Konick 2003). More recent experiments have expanded this understanding with a range of effects (Higgs et al. 2006; Arsiero et al. 2007).

Data from both simulations and from real neurons can be fit by an equation (see the Methods section) that involves a combination of the mean synaptic input that appears in the ST case and the input variance (Abbott and Chance 2005). The features of this transfer function are illustrated in Fig. 6, where we plot the output as a function of input *I* for different values of input variance. The transfer function becomes steeper as the variance decreases, indicating a gain change. We incorporate this transfer function into a network model that we call the variance dependent transfer (VDT) network. Note that the computation mechanism in this network is not simply nonlinear addition of $f(x)$ and $g(y)$, nor is it entirely direct multiplication. We therefore use the constraint we have derived to see whether the VDT network actually implements a multiplicative scheme in solving the coordinate transformation task.

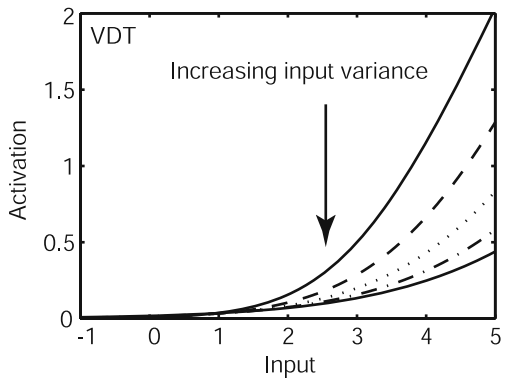

Fig. 6 The response function of Eq. (3) plotted as a function of mean input *I* for different values of input variance σ^2. Multiplicative gain modulation of the *f*–*I* is indicated by the varying slopes of the curves, which increase as the variance is decreased. The input *I* had range from −1 to 5 in increments of 0.01 and σ varied from 1 to 6 in unit increments. Parameters C_1=2 and C_2=6 (see Section 2)

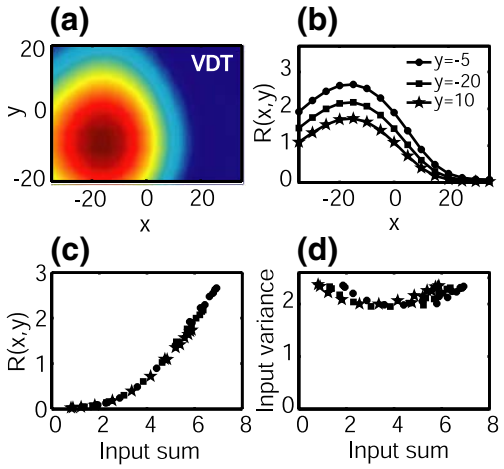

Fig. 7 (**a**) Response field of a typical unit in the hidden layer of the VDT network. (**b**) The tuning curves of the same unit show multiplicative scaling with respect to the different values of the input parameter *y* (gaze angle). (**c**) The response of the hidden unit as a function of net input. Baseline tuning curve is marked with *squares*, while the curves corresponding to the modulated responses in (**b**) are marked as *circles* and *asterisks*, respectively. (**d**) Three tuning curves mapped for different *y* values are shown with respect to their range of net inputs and input variances

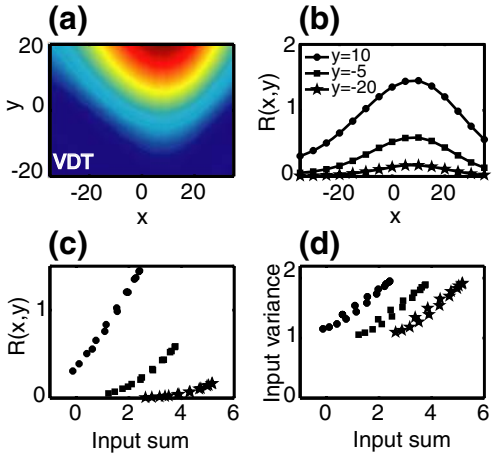

Fig. 8 Another example of a response field in the hidden layer of the VDT network. Panels are as in Fig. 7

Figures 7 and 8 show the properties of the tuning curves of two hidden units that develop in the network with VDT units. The shapes of the response field in the *x*,*y* stimulus plane is shown in panels a of both figures, while the scaling of the tuning curve with respect to the stimulus *y* is shown in panel (b). The lower two panels [(c and d)] indicate how these approximately gain modulated properties develop with respect to the transfer function. Each of the three tuning curves shown in panel (b) is defined over a different range of total input [Figs. 7(c) and 8(c)], while the range of input variances tends to stay the same across the three curves [Figs. 7(d) and 8(d)]. The tight spacing between the tuning curves in Fig. 7(b) is due to a relatively small range of input variances and tightly overlapping input ranges. On the contrary, the larger gain shifts in Fig. 8(b) are due to less overlapping input ranges and smaller variances (therefore steeper transfer functions, as shown in Fig. 6). The gain field in Fig. 7 is also less linear than that in Fig. 8.

Next we examine gain modulated in a network with ST units. Figure 9 shows the properties of the two hidden units (panels (a, b, c) and (d, e, f) respectively) in such a network. The network with ST units produces more peripheral, planar fields [Fig. 9(a) and (d)] compared to the VDT network, which tends to produce more circular response fields. The sigmoid transfer limits the activation of the hidden units to the range from 0 to 1, as opposed to VDT which has no upper bound. This limit on the activity allows for two regions of variable slope that can be used to produce gain modulation, but otherwise saturation does not appear to play a large role in the network. Approximate gain modulation arises from the use of different ranges of the transfer function for different values of *y* [Fig. 9(e) and (f)]. The key component for the gain modulation is that the net input keeps the activity away from either low- or high-activity saturation [Fig. 9(b) and c)].

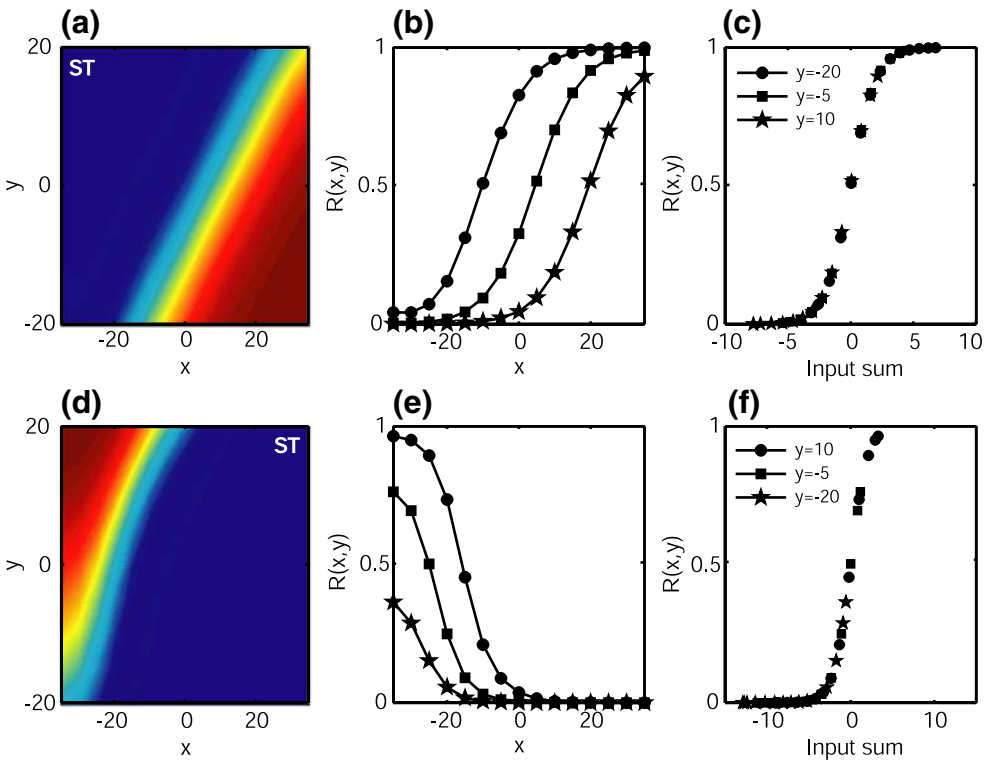

Fig. 9 (**a**) Response field of a typical unit in the hidden layer of the ST network. (**b**) The tuning curves show shifts instead of gain changes. (**c**) Tuning curves mapped plotted as a function of input to the sigmoid transfer function. (**d**) Another example of a unit from the ST network. (**e**) and (**f**) are similar to (**c**) and (**d**)

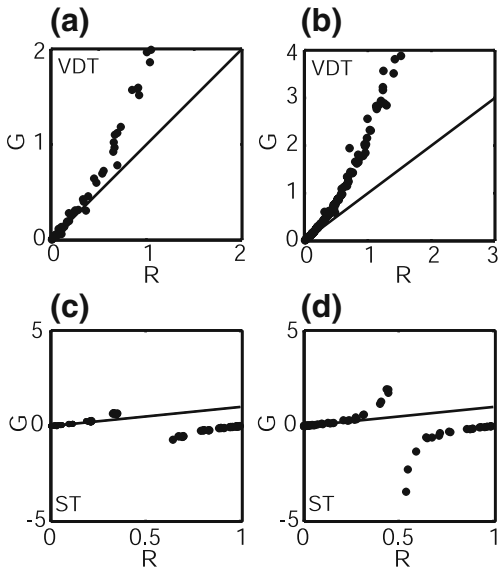

Fig. 10 (**a**) *G* vs *R* plot for the VDT network unit from Fig. 7 measure on a 15×9 grid. (**b**) *G* vs *R* plot for the VDT network unit from Fig. 8 (15×9 grid). (**c**) *G* vs *R* plot for the ST unit from Fig. 9(a) (15×9 grid). (**d**) *G* vs *R* plot for the ST unit from Fig. 9(d) (15×9 grid). The firing rates *R* are still expressed in generic scale as obtained from the neural networks

3.4 Testing the constraint on response fields of network neurons

We now investigate the *G* vs *R* properties of the units shown in Figs. 7, 8 and 9. Figure 10(a) and (b) shows (and the Wilcoxon test verifies) that both VDT and ST units look multiplicative at low firing rates, although for the unit shown in Fig. 10(b) this range was quite limited. The failure of the VDT units to be multiplicative at high rate follows from the fact that gain modulation through input variance, the mechanism being used here, fails at high firing rates (Chance et al. 2002). The departure from direct multiplication for the two ST units shown in Fig. 10(c) and (d) is even more dramatic. To check whether the VDT network was taking advantage of its multiplicative capability in a significant way, we tested networks of VDT units solving the task while holding their variances fixed. The results were not very different than those shown in Fig. 10(a) and (b), indicating that direct multiplication is not playing a large role, consistent with the deviations from multiplicative behavior seen in these figures.

4 Discussion

We have addressed the question of how to distinguish between directly multiplicative and nonlinear additive mechanisms of gain modulation on the basis of response fields or tuning curves. We showed how the ambiguity between the two mechanisms of gain modulation might be resolved by examining a constraint satisfied by the response fields in the DM case where data lies along the diagonal in the *G* vs *R* plot [Fig. 2(b) and (d)] for all ranges of the input parameters. On the contrary, NA functions (*F*) only approximate this in cases for which $(F')^2 \big/ F'' \approx F$. In most cases, numerical calculation of the ratio of derivatives of the response fields distinguishes between these two forms of the neuronal computation. The applicability of this method was tested using noisy simulated data and limited numbers of response field measurements. Provided that a high firing-rate neuron and multi-target task design is used, the resolution necessary to investigate direct multiplication is within experimental reach.

In networks with ST functions (Smith and Crawford 2005; Xing and Andersen 2000; Zipser and Andersen 1988), gain modulation arises from a nonlinear additive mechanism, similar to our discussion of the single power-law transfer neuron. Gain changes in these networks are produced by shifting the point around which the neuron operates to a portion of the *f–I* curve with a different slope. Gain modulation thus arises because the learning rule or network architecture is able to perform the appropriate operating-point shifts. The second network we studied, the VDT network, has an *f–I* transfer function that depends on the variance of the input to a neuron (Tuckwell 1988; Mel 1993; Doiron et al. 2001; Chance et al. 2002; Gabbiani et al. 2002; Mitchell and Silver 2003; Prescott and De Konick 2003). Approximate gain modulation between $f(x)$ and $g(y)$ could arise here from a transfer function which in itself contains multiplicative interaction between the net input and its variance. However, the VDT network appears to have solved the coordinate transformation task without making substantial use of this capacity. As a result, both the ST and VDT mechanisms show deviations from directly multiplicative interactions, as indicated by the *G* vs *R* plots in Fig. 10. Thus, in tests applied to real data, the mathematical constraint we have derived can only provide an indication that a multiplicative mechanism is present if it is actually being used. In such cases, it should provide a useful probe into how networks compute.

Acknowledgments We thank Gary Gibbons for helpful suggestions and T. Yao and V. Shcherbatyuk for the administrative and technical support. This work was supported by the James G. Boswell Foundation, the National Eye Institute, the Swartz Centers for Theoretical Neurobiology, NSF grant IBN-0235463 and an NIH Director's Pioneer Award, part of the NIH Roadmap for Medical Research, through grant number 5-DP1-OD114-02.

References

Abbott, L. F., & Chance, F. S. (2005). Drivers and modulators from push–pull and balanced synaptic input. *Progress in Brain Research*, *49*, 147–155.

Albrecht, D. G., & Geisler, W. S. (1991). Motion selectivity and the contrast-response function of simple cells in the visual cortex. *Visual Neuroscience*, *7*, 531–546.

Andersen, R. A., & Mountcastle, V. B. (1983). The influence of the angle of gaze upon the excitability of the light-sensitive neurons of the posterior parietal cortex. *Journal of Neuroscience*, *3*, 532–548.

Andersen, R. A., Essick, G. K., & Siegel, R. M. (1985). The encoding of spatial location by posterior parietal neurons. *Science*, *230*, 456–458.

Arsiero, M., Lüscher, H. R., Lundstrom, B. N., & Giugliano, M. (2007). The impact of input fluctuations on the frequency–current relationship of layer 5 pyramidal neurons in the rat medial prefrontal cortex. *Journal of Neuroscience*, *27*, 3274–3284.

Bishop, C. M. (1995). *Neural networks for pattern recognition*.. Oxford, New York: Oxford University Press.

Bremmer, F., Ilg, U. J., Thiele, A., Distler, C., & Hoffmann, K. P. (1997). Eye position effects in monkey cortex. I. Visual and pursuit-related activity in extrastriate areas MT and MST. *Journal of Neurophysiology*, *77*, 944–961.

Carandini, M., & Ferster, D. (2000). Membrane potential and firing rate in cat primary visual cortex. *Journal of Neuroscience*, *20*, 470–484.

Carandini, M., Heeger, D. J., & Movshon, J. A. (1997). Linearity and normalization in simple cells of the macaque primary visual cortex. *Journal of Neuroscience*, *17*, 8621–8644.

Chance, F. S., Abbott, L. F., & Reyes, A. D. (2002). Gain modulation from background synaptic input. *Neuron*, *35*, 773–782.

Cohen, Y. E., & Andersen, R. A. (2000). Eye position modulates reach activity to sounds. *Neuron*, *27*, 647–652.

Doiron, B., Longtin, A., Berman, N., & Maler, L. (2001). Subtractive and divisive inhibition: Effect of voltage-dependent inhibitory conductances and noise. *Neural Computation*, *13*, 227–248.

Gabbiani, F., Krapp, H. G., Koch, C., & Laurent, G. (2002). Multiplicative computation in a visual neuron sensitive to looming. *Nature*, *420*, 320–324.

Galletti, C., & Battaglini, P. P. (1989). Gaze-dependent visual neurons in area V3A of monkey prestriate cortex. *Journal of Neuroscience*, *9*, 1112–1125.

Gardner, J. L., Anzai, A., Ohzawa, I., & Freeman, R. D. (1999). Linear and nonlinear contributions to orientation tuning of simple cells in the cat's striate cortex. *Visual Neuroscience*, *16*, 1115–1121.

Groh, J. M., Trause, A. S., Underhill, A. M., Clark, K. R., & Inati, S. (2001). Eye position influences auditory responses in primate inferior colliculus. *Neuron*, *29*, 509–518.

Grunewald, A., Linden, J. F., & Andersen, R. A. (1999). Responses to auditory stimuli in macaque lateral intraparietal area. I. Effects of training. *Journal of Neurophysiology*, *82*, 330–342.

Heeger, D. J. (1992). Normalization of cell responses in cat striate cortex. *Visual Neuroscience*, *9*(2): 181–197.

Higgs, M. H., Slee, S. J., & Spain, W. J. (2006). Diversity of gain modulation by noise in neocortical neurons: Regulation by the slow afterhyperpolarization conductance. *Journal of Neuroscience*, *26*, 8787–8799.

McAdams, C. J., & Maunsell, J. H. R. (2000). Attention to both space and feature modulates neuronal responses in macaque area V4. *Journal of Neurophysiology*, *83*, 1751–1755.

Mel, B. W. (1993). Synaptic integration in an excitable dendritic tree. *Journal of Neurophysiology*, *70*, 1086–1101.

Mitchell, S., & Silver, R. (2003). Shunting inhibition modulates neuronal gain during synaptic excitation. *Neuron*, *38*, 433–445.

Murphy, B. K., & Miller, K. D. (2003). Multiplicative gain changes are induced by excitation or inhibition alone. *Journal of Neuroscience*, *23*, 10040–10051.

Murthy, A., Humphrey, A. L., Saul, A. B., & Feidler, J. C. (1988). Laminar differences in the spatiotemporal structure of simple cell receptive fields in cat area 17. *Visual Neuroscience*, *15*, 239–256.

Pouget, A., & Sejnowski, T. J. (1995). Spatial representations in the parietal cortex may use basis functions. In A. Tesauro, D. Touretzky, & T. Leen (Eds.) *Advances in neural information processing systems* (pp. 157–164). Cambridge: MIT Press.

Prescott, S. A., & De Konick, Y. (2003). Gain control of firing rate by shunting inhibition: Roles of synaptic noise and dendritic saturation. *Proceedings of the National Academy of Sciences*, *100*, 2076–2081.

Rumelhart, D. E., Hinton, G. E., & Williams, R. J. (1986). Learning internal representations by error propagation. In J. L. McClelland, & D. E. Rumelhart (Eds.) *Parallel distributed processing: Explorations in the microstructure of cognition* (pp. 318–362). Cambridge: MIT Press.

Salinas, E., & Abbott, L. F. (1996). A model of multiplicative neural responses in parietal cortex. *Proceedings of the National Academy of Sciences of the United States of America*, *93*, 11956–11961.

Salinas, E., & Abbott, L. F. (1997). Invariant visual responses from attentional gain fields. *Journal of Neurophysiology*, *77*, 3267–3272.

Salinas, E., & Their, P. (2000). Gain modulation: a major computational principle of the central nervous system. *Neuron*, *27*, 15–21.

Salinas, E., & Sejnowski, T. J. (2001). Gain modulation in the central nervous system: Where behavior, neurophysiology and computation meet. *The Neuroscientist*, *7*, 430–440.

Smith, M., & Crawford, J. (2005). Distributed population mechanism for the 3-D oculomotor reference frame transformation. *Journal of Neurophysiology*, *93*, 1742–1761.

Schwartz, O., & Simoncelli, E. P. (2001). Natural signal statistics and sensory gain control. *Nature Neuroscience*, *4*(8): 819–825.

Treue, S., & Martinez-Trujillo, J. C. (1999). Feature-based attention influences motion processing gain in macaque visual cortex. *Nature*, *399*, 575–579.

Tuckwell, H. C. (1988). Introduction to theoretical neurobiology. Cambridge: Cambridge University Press.

Xing, J., & Andersen, R. A. (2000). Models of the posterior parietal cortex which perform multimodal integration and represent space in several coordinate frames. *Journal of Cognitive Neuroscience*, *12*, 601–614.

Zipser, D., & Andersen, R. A. (1988). A back-propagation programmed network that simulates response properties of a subset of posterior parietal neurons. *Nature*, *331*, 679–684.